THE JOURNAL OF BIOLOGICAL CHEMISTRY
Vol. 277, No. 32, Issue of August 9, pp. 29242–29252, 2002
Printed in U.S.A.

Contribution of Molecular Modeling and Site-directed Mutagenesis to the Identification of Two Structural Residues, Arg-220 and Asp-227, in Aminopeptidase A*

Received for publication, May 6, 2002
Published, JBC Papers in Press, May 30, 2002, DOI 10.1074/jbc.M204406200

Raphaël Rozenfeld‡, Xavier Iturrioz‡, Bernard Maigret§, and Catherine Llorens-Cortes‡¶

From ‡INSERM, Unité 36, Collège de France, 11, place Marcelin Berthelot, 75005 Paris and §CNRS, Unité Mixte de Recherche 7565, Laboratoire de Chimie Théorique, Université de Nancy, 54506 Vandoeuvre-les-Nancy, France

Aminopeptidase A is a zinc metalloenzyme involved in the formation of brain angiotensin III, which exerts a tonic stimulatory action on the central control of blood pressure. Thus, central inhibitors of aminopeptidase A constitute putative central antihypertensive agents. Mutagenic studies have been performed to investigate organization of the aminopeptidase A active site, with a view to designing such inhibitors. The structure of one monozinc aminopeptidase (leukotriene A_4 hydrolase) was recently resolved and used to construct a three-dimensional model of the aminopeptidase A ectodomain. This new model, highly consistent with the results of mutagenic studies, showed a critical structural interaction between two conserved residues, Arg-220 and Asp-227. Mutagenic replacement of either of these two residues disrupted maturation and subcellular localization and abolished the enzymatic activity of aminopeptidase A, confirming the critical structural role of these residues. In this study, we generated the first three-dimensional model of a strict aminopeptidase, aminopeptidase A. This model constitutes a new tool to probe further the active site of aminopeptidase A and to design new inhibitors of this enzyme.

Aminopeptidase A (APA[1]; EC 3.4.11.7) is a 160-kDa homodimeric type II membrane-bound aminopeptidase that specifically cleaves the N-terminal glutamyl or aspartyl residue from peptide substrates such as angiotensin II and cholecystokinin-8 *in vitro* (1, 2). APA is present in many tissues, particularly in the brush border of intestinal and renal epithelial cells and in the vascular endothelium (3). APA and other components of the brain renin-angiotensin system (4) have been identified in several brain nuclei involved in the control of body fluid homeostasis and cardiovascular functions. Studies with specific and selective APA inhibitors (5) have shown that, *in vivo*, APA converts brain angiotensin II to angiotensin III (6) and that brain angiotensin III exerts a tonic stimulatory action on the central control of blood pressure (7). Thus, the central administration of APA inhibitors results in a large decrease in arterial blood pressure in alert spontaneously hypertensive rats (7), suggesting that brain APA is a putative central therapeutic target for the treatment of hypertension (reviewed in Ref. 8).

Determination of the complete amino acid sequence of APA in mouse (9), human (10, 11), rat (12), and pig (13) has revealed the presence of the consensus sequence HE*XX*H, which is found in the zinc metalloprotease family, the zincins (14, 15). In the absence of structural data on monozinc aminopeptidases, site-directed mutagenesis studies based on alignment of the sequence of APA with those of other monozinc aminopeptidases were used to probe the organization of the APA active site. These studies resulted in the identification of several residues involved in zinc coordination (16, 17), catalysis (17, 18), and substrate binding (19). Some of these conserved residues were also recently identified in other related aminopeptidases such as thyrotropin-releasing hormone-degrading enzyme (EC 3.4.19.6) (20), aminopeptidase N (EC 3.4.11.2) (21), leukotriene A_4 hydrolase (LTA_4H; EC 3.3.2.6) (22, 23), and insulin-regulated membrane aminopeptidase (EC 3.4.11.3) (24). On the basis of our data, we proposed a model for the organization of the active site of APA and a putative catalytic mechanism for this enzyme (25) similar to that proposed for thermolysin on the basis of x-ray diffraction studies (26). According to this model, in the absence of substrate, the zinc atom is tetracoordinated by three zinc ligands (His-385, His-389, and Glu-408) and a water molecule. When the substrate enters the active site, its recognition and orientation are ensured by interactions with several residues. First, in the S1 subsite, which recognizes only N-terminal acidic residues, Ca^{2+} interacts with the P1 carboxylate side chain of the substrate. In the anionic binding site, Glu-352 interacts with the free N-terminal part of the substrate. The zinc atom is simultaneously hexacoordinated by establishing two additional interactions with the carbonyl group of the scissile peptide bond and the unprotonated α-amino group of the substrate. The negative charge of Glu-386 polarizes the zinc-coordinated water molecule and promotes its nucleophilic attack on the carbonyl carbon of the peptide bond to be cleaved. The resulting tetrahedral intermediate is stabilized by electrostatic interactions with the zinc ion and hydrogen bonds with Glu-386, Tyr-471, and Glu-352. Finally, the transfer of a proton from Glu-386 to the leaving nitrogen of the scissile peptide bond triggers the cleavage of the peptide bond and the release of the products.

Determination of the x-ray crystal structure of LTA_4H/aminopeptidase, a bifunctional enzyme, recently revealed the crucial role of certain residues in zinc coordination, exopeptidase specificity, and catalytic activity (27). The roles of these residues are similar to those of their counterparts in

* The costs of publication of this article were defrayed in part by the payment of page charges. This article must therefore be hereby marked "*advertisement*" in accordance with 18 U.S.C. Section 1734 solely to indicate this fact.

¶ To whom correspondence should be addressed. Tel.: 33-1-44-27-1663; Fax: 33-1-44-27-1691; E-mail: c.llorens-cortes@college-de-france.fr.

[1] The abbreviations used are: APA, aminopeptidase A; LTA_4H, leukotriene A_4 hydrolase; GluNA, α-L-glutamyl-β-naphthylamide; MD, molecular dynamics; CHO, Chinese hamster ovary; PNGase F, peptide *N*-glycosidase F; Endo H, endoglycosidase H; PBS, phosphate-buffered saline; CHAPS, 3-[(3-cholamidopropyl)dimethylammonio]-1-propanesulfonic acid; ER, endoplasmic reticulum.

APA, as previously determined by site-directed mutagenesis. We then carried out computer-assisted modeling of APA using the crystal structure of LTA_4H as a template and the functional data collected from our previous site-directed mutagenesis studies. We constructed a three-dimensional model of the APA ectodomain from residues 79 to 559; this domain surrounds the zinc-binding domain. We subsequently docked the specific and selective APA inhibitor glutamate phosphonate (28) into the active site. This made it possible to produce, for the first time, a three-dimensional representation of a strict (*i.e.* monofunctional) monozinc aminopeptidase and of the interactions between the active site and the inhibitor glutamate phosphonate, an analog of the transition state, thereby reproducing the interactions between the substrate and the enzyme that occur during catalysis. This new model will be useful for further investigation of the organization of the APA active site and for the definition of a pharmacophore of the APA inhibitor, a powerful tool for the design of specific and selective inhibitors for use as central antihypertensive agents.

In this model, we identified a salt bridge interaction between two strictly conserved residues, Arg-220 and Asp-227. This interaction appears to be necessary for cohesion of the N-terminal β-sheet domain and therefore for correct folding of the N-terminal domain surrounding the active site. We used site-directed mutagenesis to validate our model by confirming the functional role of these residues. We replaced Arg-220 with alanine and aspartate and Asp-227 with alanine and arginine and inverted the two residues. We then characterized the maturation, trafficking, and enzymatic activity of the recombinant wild-type and mutant APAs.

EXPERIMENTAL PROCEDURES

Materials

Restriction endonucleases and DNA-modifying enzymes were obtained from New England Biolabs Inc. (Hitchin, England) and were used according to the manufacturer's instructions. The Expand high-fidelity *Taq* polymerase PCR system was purchased from Roche Molecular Biochemicals (Mannheim, Germany). The liposomal transfection reagent LipofectAMINE, the pcDNA3.1-His vector, and the anti-Xpress antibody were purchased from Invitrogen (Groningen, The Netherlands). The anti-His_5 antibody was purchased from QIAGEN Inc. Immobilized cobalt affinity columns (Talon) were obtained from CLONTECH (Heidelberg, Germany). The synthetic substrate α-L-glutamyl-β-naphthylamide (GluNA) was purchased from Bachem (Bunderdorf, Switzerland).

Methods

Modeling of APA—As no experimentally determined three-dimensional structure is yet available for APA, we constructed a three-dimensional model by homology modeling. The recently published x-ray crystallographic structure of human LTA_4H (27) was used as the template, and Accelrys homology software was used to construct the model for APA. The correct alignment of the human LTA_4H and mouse APA sequences was determined from multiple sequence alignments between several proteins of this family and experimental information obtained in previous site-directed mutagenesis studies on APA carried out in our laboratory (17–19, 25, 29). A preliminary model was obtained from the transfer of coordinates from LTA_4H to APA in the aligned regions. The model was completed by adding the missing loops connecting the moieties already obtained. The APA model obtained therefore concerned only residues 79–539, corresponding to the region most highly conserved between APA and LTA_4H (31% similarity). We were unable to identify suitable templates for modeling the remaining C-terminal APA sequence and therefore present here a model covering only residues 79–539. However, this part of the APA protein seems to be the most important, at least as far as enzymatic activity is concerned.

The preliminary three-dimensional $3\text{-}D^0$ model obtained by the crude transfer of coordinates from LTA_4H to APA on the basis of homology was then surrounded by a shell of 2700 water molecules to take into account the effect of the surrounding solvent during the refinement procedure. The refinement procedure consisted of several energy minimization steps carried out by the conjugate gradient method. We began by fixing the backbone of the protein such that only the protein side chains and water molecule movements were variable. Next, the whole system was relaxed. All Arg, Lys, Asp, and Glu side chains were considered ionic, and a 20-Å cutoff point was used to truncate non-bonded interactions. The dielectric constant was 1. We used the Accelrys CFF97 force field, as this class II force field provided all the necessary parameters for calculating all Zn^{2+} interactions with other groups in the system.

The resulting $3\text{-}D^1$ model was then subjected to another refinement procedure including several rounds of energy minimization (until convergence) and short molecular dynamics (MD) runs (100 ps at 300 K). This process was carried out to check the stability of the model over time.

We checked the consistency of the $3\text{-}D^2$ model obtained at the end of these calculations, especially in the active-site region (according to several geometric requirements concerning the zinc atom coordination shell) and the water shell region. It appeared that many water molecules escaped from the shell that initially surrounded the protein, creating several ionic groups that were exposed to others without their solvation shell. This resulted in modification of the exposed active-site configuration and therefore of zinc atom coordination. We therefore decided to restart from the $3\text{-}D^1$ system, placed within a 85-$Å^3$ water box, and to carry out the refinement procedure described above (minimization + MD). At this stage, the system consisted of the protein and 16,886 water molecules. Periodic boundary conditions were used with the same cutoff point as before. The resulting $3\text{-}D^3$ model was used in all subsequent calculations.

We carried out docking calculations in the $3\text{-}D^3$ model using as ligands the selective APA inhibitor glutamate phosphonate, bestatin, and glutamate-thiol. The inhibitors were introduced according to the position of bestatin in LTA_4H. Three models were built in this way. Each protein + ligand + solvent box was then relaxed step by step, until all the degrees of freedom were considered in the minimization and MD processes. After several steps of energy minimization + 100-ps MD + energy minimization, the three models were considered to be stable, as the residual mean square deviations between the C^α atoms of the starting structure and the final structure were <1 Å. We also checked the stability of the $3\text{-}D^3$ model by replacing Arg-220 and Asp-227 with alanines and performing supplementary MD runs. All the preliminary calculations were performed on SGI O2 workstations, and the heaviest calculations were performed at the Centre Informatique National de l'Enseignement Superieur (CINES) supercomputing center on an Origin 3800.

Cloning and Site-directed Mutagenesis— The mouse cDNA encoding APA was inserted into the expression vector pcDNA3.1-His (29), and mutants were generated by PCR-based site-directed mutagenesis as previously described (30). Two overlapping regions of the cDNA were amplified separately using two flanking oligonucleotides, oligonucleotide A (5′-TTAATACGACTCACTATAGGGA-3′, bp 862–883) as a forward primer and oligonucleotide B (5′-GAATCCTAAGATAGAGGCCCGGAG)-3′, bp 3215–3238) as a reverse primer, and two overlapping oligonucleotides containing the mutated residues (C1D1 for Ala-220, C2D2 for Asp-220, C3D3 for Ala-227, C4D4 for Arg-227, C5D5 for Asp-220/Arg-227, and C6D6 for Ala-221). The forward primers were as follows: C1, 5′-ACAGATGCCGCGAAGTCCTTC-3′; C2, 5′-ACAGATGCCGACAAGTCCTTC-3′; C3, 5′-CCTTGTTTCGCAGAACCCAAC-3′; C4, 5′-CCTTGTTTCCGAGAACCCAAC-3′; C5, 5′-ACAGATGCCGACAAGTCCTTCCCTTGTTTCAGGGAACCCAAC; and C6, 5′-GATGCCAGGGCGTCCTTCCCT-3′. The reverse primers were as follows: D1, 5′-GAAGGACTTCGCGGCATCTGT-3′; D2, 5′-GAAGGACTTGTCGGCATCTGT-3′; D3, 5′-GTTGGGTTCTGCGAAACAAGG-3′; D4, 5′-GTTGGGTTCTCGGAAACAAGG-3′; D5, 5′-GTTGGGTTCCCTGAAACAAGGGAAGGACTTGTCGGCATCTGT-3′; and D6, 5′-AGGGAAGGACGCCCTGGCATC-3′. The underlined bases encode the new amino acid residue replacing arginine at position 220 (C1, C2, D1, and D2), aspartate at position 227 (C3, C4, D3, and D4), Arg-220 and Asp-227 (C5 and D5), and lysine at position 221 (C6 and D6). Nucleotide numbering is as for the mouse APA sequence (9) deposited in the GenBank™/EBI Data Bank (accession number M29961).

The products of the first two amplifications (A-D1–6 and B-C1–6) were used as the template for a second PCR with the two flanking oligonucleotides A and B. For all PCRs, high-fidelity *Taq* polymerase (1 unit) was used (25 cycles at 94 °C for 30 s, 54 °C for 45 s, and 72 °C for 2 min). The final 2376-bp PCR product was digested with *Hin*dIII and *Eco*RV, and the resulting 1505-bp *Hin*dIII-*Eco*RV fragment containing the mutation was used to replace the corresponding non-mutated region (*Hin*dIII-*Eco*RV) of the full-length APA cDNA. The

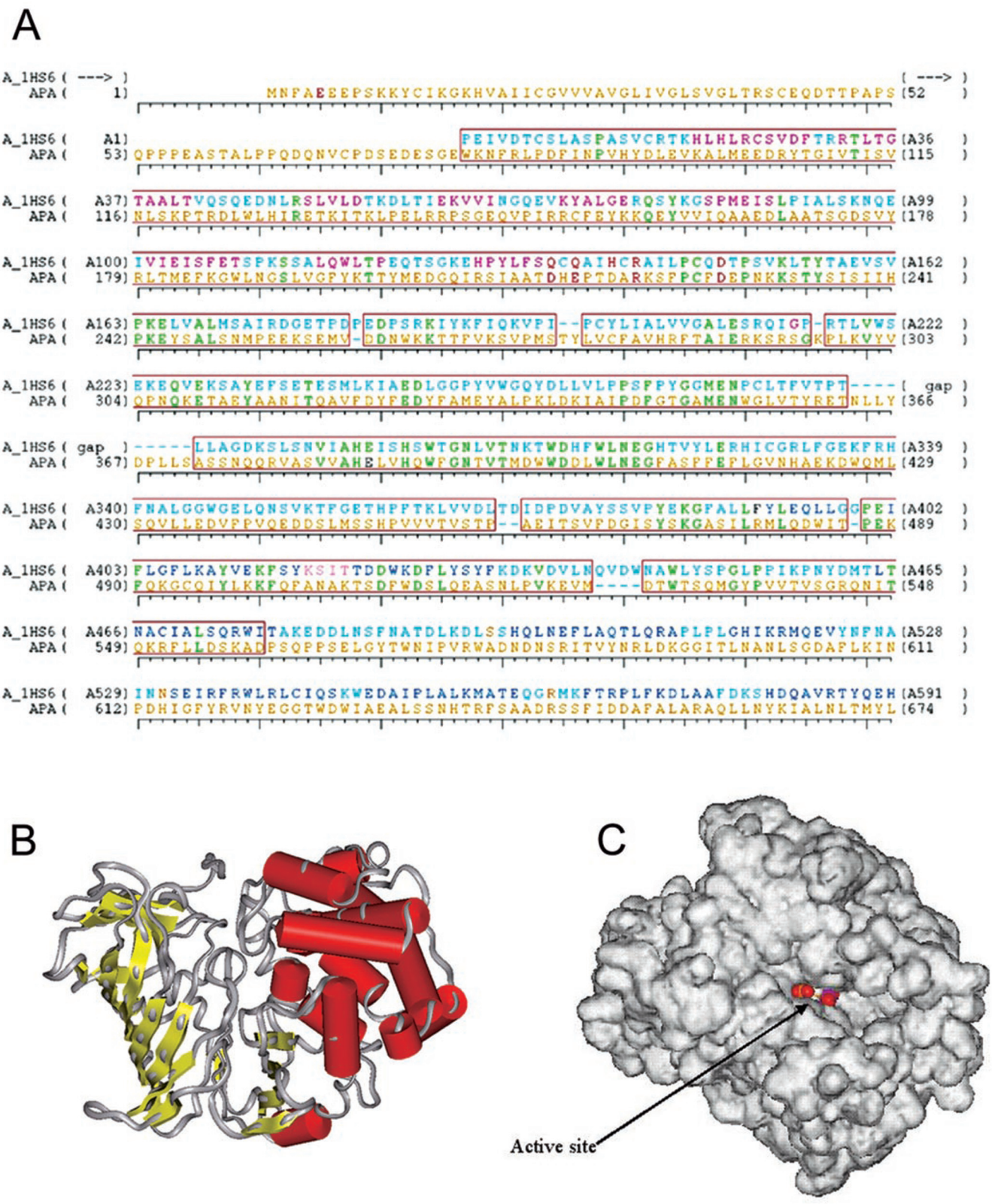

FIG. 1. **Modeling of APA by homology using LTA_4H as a template.** *A*, sequence alignment between APA and LTA_4H used for homology modeling of APA. The correct alignment of the human LTA_4H (*A_1HS6*) and mouse APA sequences was determined from multiple sequence alignments between several proteins of this family and experimental information obtained in previous site-directed mutagenesis studies. *B*, C^{α} ribbon diagram of the tertiary structure of APA. The protein is organized in three domains: the N-terminal domain consisting mainly of β-sheets (represented as *yellow arrows*), the globular active-site domain, and the C-terminal helical domain (*red cylinders*). *C*, molecular surface of the APA model showing the cavity for ligand positioning.

presence of the mutation and the absence of nonspecific mutations were confirmed by automated sequencing on an Applied Biosystems 377 DNA Sequencer with dye deoxy terminator chemistry.

Cell Culture, Establishment of Stable CHO-K1 Cell Lines Producing Wild-type His-APAs, and Purification of Recombinant Wild-type His-APA—CHO-K1 cells (American Type Culture Collection, Manassas,

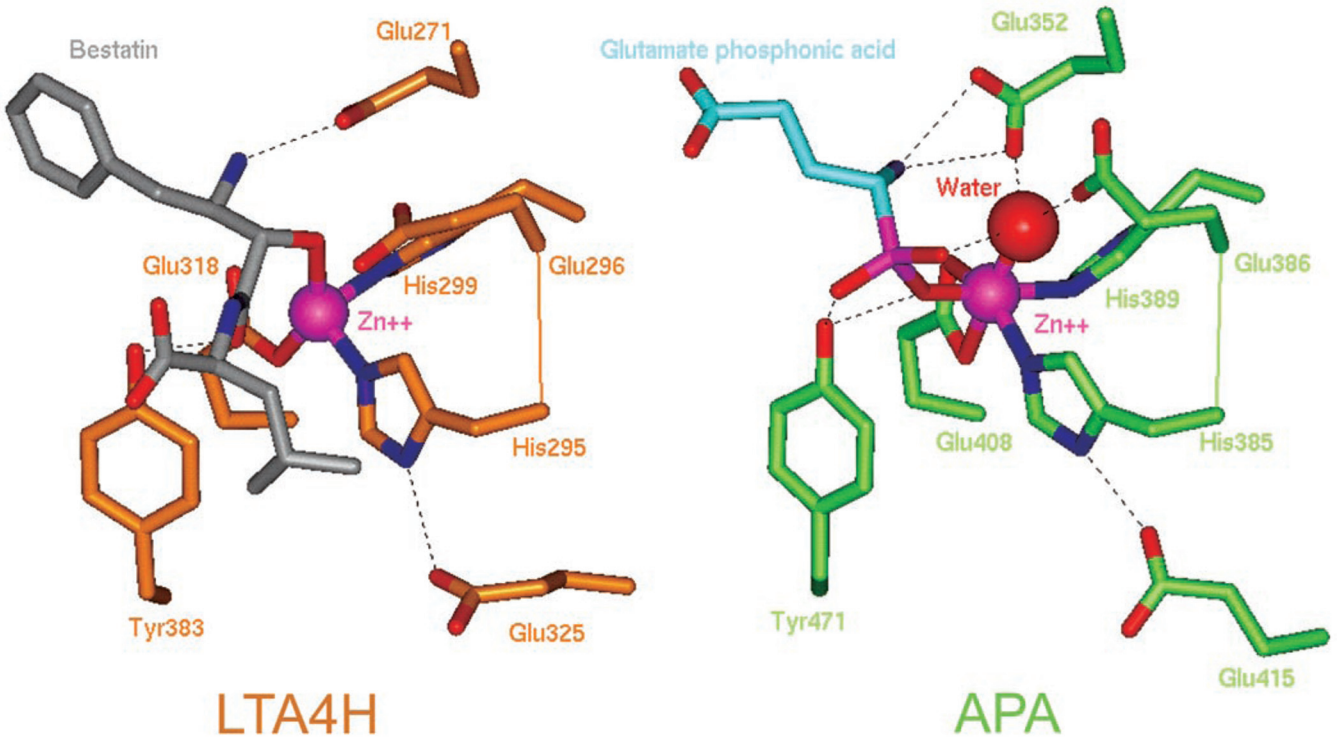

FIG. 2. **Comparison of the active-site organization in the LTA_4H template and in the APA model.** LTA_4H is colored in *orange*, and APA is colored in *green*. The water molecule coordinated to the zinc ion (*purple sphere*) is represented as a *red sphere* in the APA active site. The carbon atoms of bestatin, the inhibitor docked in the LTA_4H active site, are colored in *gray*, whereas the carbon atoms of glutamate phosphonate, the inhibitor docked in the APA active site, are colored in *light blue*.

VA) were maintained in Ham's F-12 medium supplemented with 7% fetal calf serum, 0.5 mM glutamine, 100 units/ml penicillin, and 100 μg/ml streptomycin (all from Roche Molecular Biochemicals). A stable cell line producing polyhistidine-tagged wild-type APA was established as previously described (29). Stably transfected CHO cells were harvested, and a crude membrane preparation was obtained as previously described (29). Wild-type His-APA was purified from the solubilized crude membrane preparation by metal affinity chromatography with a metal chelate resin column (Talon-Co^{2+}) as previously described (29). The purity of the final preparation was assessed by SDS-PAGE on 7.5% polyacrylamide gels as described by Laemmli (31). Proteins were stained with Coomassie Brilliant Blue R-250. Protein concentrations were determined by the Bradford assay using bovine serum albumin as the standard (42).

Metabolic Labeling and Immunoprecipitation—CHO cells were transfected with 1 μg of the plasmid containing either wild-type or mutant His-APA cDNA using LipofectAMINE Plus (Invitrogen) according to the manufacturer's protocol. A population of cells enriched in transiently transfected cells was selected for resistance to 750 μg/ml Geneticin (G418) over a 10-day period. These resistant cells (300,000 cells/well) were then incubated for 30 min in methionine/cysteine serum-free Ham's F-12 medium supplemented with 100 μCi/ml [^{35}S]methionine/cysteine (pulse). The cells were then incubated for various lengths of time (0, 90, and 180 min) in serum-free Ham's F-12 medium (chase). The cell medium was discarded; the cells were harvested; and proteins were solubilized by incubation overnight at 4 °C with 600 μl of 50 mM Tris-HCl (pH 7.4), 150 mM NaCl, 10 mM EDTA, and 1% (v/v) Triton X-100. The resulting lysate was centrifuged at 20,000 $\times$ *g* for 5 min at 4 °C to remove the insoluble material. The supernatant was incubated with the mouse monoclonal anti-His_5 antibody (5 μl, 1 μg) and protein A-Sepharose (50% (w/v) suspension in solubilization buffer; Amersham Biosciences) for 2 h at 4 °C for immunoprecipitation. The immune complexes were collected by centrifugation and washed four times with solubilization buffer and once with 20 mM Tris-HCl (pH 6.8). Proteins were eluted by boiling in 25 μl of Laemmli buffer and resolved by 5% SDS-PAGE as described by Laemmli (31). The gel was dried and placed against x-ray film for autoradiography.

Peptide N-Glycosidase F and Endoglycosidase H Treatment—A population of CHO cells enriched in transiently transfected cells producing wild-type and mutant His-APAs was subjected to a 30-min pulse and a 90-min chase. The cells were lysed, and the proteins were solubilized and immunoprecipitated. The samples were washed and centrifuged as described above. The immune complexes were then eluted by boiling for 15 min in 100 μl of denaturing buffer (0.01% SDS). The samples were incubated with or without 5 milliunits of peptide *N*-glycosidase F (PNGase F; Roche Molecular Biochemicals) at pH 9 for 18 h at 37 °C or 1 unit of endoglycosidase H (Endo H; Roche Molecular Biochemicals) at pH 6 for 18 h at 37 °C. The reaction was stopped by adding Laemmli buffer, and the samples were subjected to SDS-PAGE on 5% acrylamide gels, which were then dried and placed next to x-ray film for autoradiography.

Immunofluorescence and Double Labeling of Transiently Transfected CHO Cells—CHO cells were seeded (25,000 cells) on 14-mm diameter coverslips and transiently transfected with constructs encoding wild-type and mutant His-APAs. The cells were cultured for 48 h in Ham's F-12 medium in a humidified atmosphere of 5% CO_2 and 95% air. They were then incubated with cycloheximide (70 μM) in Ham's F-12 medium for 90 min, fixed, and permeabilized by incubation for 5 min in 100% ice-cold methanol. The cells were rinsed three times in 0.1 M phosphate-buffered saline (PBS) (pH 7.4) and then saturated by incubation with 5% bovine serum albumin for 30 min at room temperature. They were incubated with a 1:500 dilution of rabbit polyclonal anti-rat APA serum (32), a kind gift from Dr. S. Wilk, in PBS and 2% bovine serum albumin for 2 h at room temperature. The coverslips were washed three times with cold PBS and then incubated with a 1:500 dilution of cyanin-3-conjugated polyclonal anti-rabbit antibody in PBS and 2% bovine serum albumin for 2 h at room temperature. The coverslips were washed four times with PBS and mounted in Mowiol (Sigma) for confocal microscopy. For double labeling, fluorescein-conjugated concanavalin A (50 μg, 1:100) was added together with the secondary antibody. Transiently transfected AtT20 cells were analyzed by evaluating immunofluorescence under the same conditions.

Cells were examined with a Leica TCS SP II confocal laser scanning microscope equipped with an argon/krypton laser and configured with a Leica DM IRBE inverted microscope. Cyanin-3 fluorescence was detected after 100% excitation at 568 nm. For double detection of cyanin-3 and fluorescein, fluorescence was assessed after 100% excitation at 568 nm and 100% excitation at 488 nm, respectively. Fluorescence was detected in windows of 580–630 and 500–550 nm. Images (1024 $\times$ 1024 pixels) were obtained with a $\times$63 magnification oil-immersion objective. Each image corresponded to a cross-section of the cell.

Enzyme Assay—For both protein concentration determination and

A

```
                                  220   227                                  386
APA mouse        DGQIRSIAATDHEPTDARKSFPCFDEPNKKSTYSISIIHPKEYSAL----135----AHELVHQWFGNTVTMDWWDDLWLNEGFASFFEFLGVNHAE
APA human        NGRVKSIAATDHEPTDARKSFPCFDEPNKKATYTISITHPKEYGAL----135----AHELVHQWFGNIVTMDWWEDLWLNEGFASFFEFLGVNHAE
APN rat          GGNKKVVATTQMQAADARKSFPCFDEPAMKASFNITLIHPNNLTAL----137----AHELAHQWFGNLVTVDWWNDLWLNEGFASYVEFLGADYAE
APN human        GNVRKVVATTQMQAADARKSFPCFDEPAMKAEFNITLIHPKDLTAL----140----AHELAHQWFGNLVTIEWWNDLWLNEGFASYVEYLGADYAE
APN mouse        GDVKKVVATTQMQAADARKSFPCFDEPAMKAMFNITLIYPNNLIAL----139----AHELAHQWFGNLVTVDWWNDLWLNEGFASYVEFLGADYAE
IRAP rat         SNEKKNFAATQFEPLAARSAFPCFDEPAFKATFIIKITRDEHHTAL----134----AHELAHQWFGNLVTMQWWNDLWLNEGFATFMEYFSVEKIF
PSA mouse        AGEVRYAAVTQFEATDPRRAFPCWDEPAIKATFDISLVVPKDRVAL----137----GHELAHQWFGNLVTMEWWTHLWLNEGFASWIEYLCVDHCF
LTA4H rat        SGKQHPYLFSQWEAIHCRAILPCQDT-SVKLTYTAEVSVPKELVAL----124----AHEISHSWTGNLVTNKTWDHFWLNEGHTVYLERHICGRLF
LTA4H mouse      SGKQHPYLFSQCQAIHCRAILPCQDTPSVKLTYTAEVSVPKELVAL----124----AHEISHSWTGNLVTNKTWDHFWLNEGHTVYLERHICGRLF
LTA4H human      SGKEHPYLFSQCQAIHCRAILPCQDTPSVKLTYTAEVSVPKELVAL----124----AHEISHSWTGNLVTNKTWDHFWLNEGHTVYLERHICGRLF
APB rat          AGKKKPFVYTQGQAVLNRAFFPCFDTPAVKCTYSALVEVPDGFTAV----119----IHEISHSWFGNLVTNANWGEFWLNEGFTMYAQRRISTILF
```

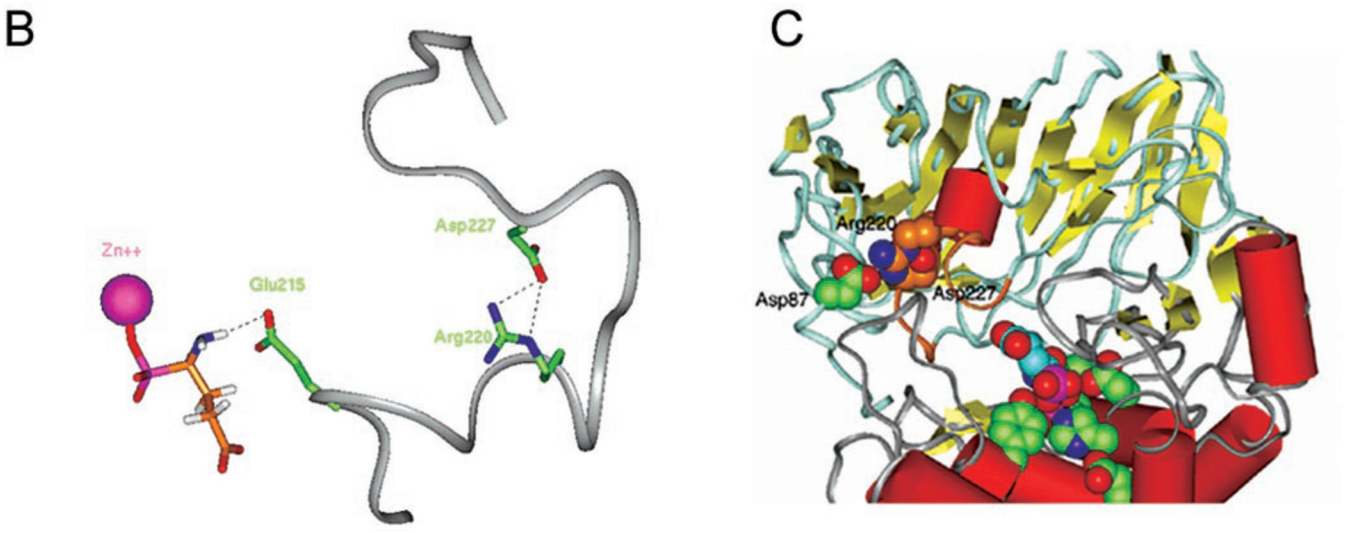

FIG. 3. **Arg-220 and Asp-227, two residues conserved in monozinc aminopeptidases, play an important role in the structure of APA.** *A*, alignment of the mouse APA amino acid sequence with sequences of other monozinc aminopeptidases. The consensus zinc-binding motif HE*XX*H is indicated in *italics*; the conserved residues Arg-220 and Asp-227 in APA and their homologous residues in other sequences are indicated in *boldface*. Shown is the alignment of the amino acid sequences of mouse and human APA (EC 3.4.11.7); rat, human, and mouse aminopeptidase N (*APN*; EC 3.4.11.2); rat insulin-regulated membrane aminopeptidase (*IRAP*; EC 3.4.11.3); mouse puromycin-sensitive aminopeptidase (*PSA*; EC 3.4.11.14); rat, mouse, and human LTA_4H (EC 3.3.2.6); and rat aminopeptidase B (*APB*; EC 3.4.11.6). *B*, C^{α} ribbon representation of the loop organization between residues 215 and 230 and the Arg-220–Asp-227 salt bridge interaction that maintains the hairpin. The Glu-215 side chain interacting with the inhibitor glutamate phosphonate is also depicted. *C*, C^{α} ribbon diagram showing the position of the Arg-220–Asp-227 salt bridge (colored in *orange*) inside the N-terminal β-sheet domain. The Asp-87 residue participating in the Asp-87–Arg-220–Asp-227 triad is shown as *green* Corey-Pauling-Koltun atoms. The active-site residues and the inhibitor glutamate phosphonate are also represented (*green* and *light blue* Corey-Pauling-Koltun atoms, respectively).

GluNA hydrolysis, purified recombinant wild-type His-APA and either solubilized untransfected or transiently transfected CHO cells producing wild-type or mutant APAs were used. Wild-type His-APA was purified as described above. Untransfected cells and cells transiently expressing mutant His-APAs (300,000 cells) were harvested and solubilized by incubation overnight in 400 μl of 0.5% CHAPS in Tris-HCl (pH 7.4).

Protein Concentration Determination—The Bradford assay was used for purified wild-type His-APA and solubilized cells using bovine serum albumin as a standard to determine the total protein concentration of the samples. Dot blots were then used to determine the concentration of His-APA in the solubilized samples. A standard curve was generated by spotting various amounts of purified His-APA on a nitrocellulose membrane. We then spotted equivalent amounts of total protein for each of the solubilized samples. Untransfected CHO cells were used to identify nonspecific immunoreactivity in the solubilized cells. Dot blots of recombinant APAs were analyzed with a monoclonal anti-Xpress antibody (1:5000 dilution). Immunoreactive material was detected with a horseradish peroxidase-conjugated anti-mouse antibody (1:20,000 dilution) and developed by enhanced chemiluminescence (ECL, Amersham Biosciences, Buckinghamshire, England). Chemiluminescence was measured by microdensitometric scanning of the dot blots. The concentrations of mutant His-APAs were calculated from the purified His-APA standard curve.

GluNA Hydrolysis—The activities of the wild-type and mutant His-APAs were determined by monitoring the rate of hydrolysis of a synthetic substrate (GluNA) as previously described (33). Recombinant His-APAs were incubated at 37 °C in the presence of 5×10^{-4} M GluNA and 4 mM $CaCl_2$ in a final volume of 100 μl of 50 mM Tris-HCl (pH 7.4). Bestatin, a nonspecific aminopeptidase inhibitor, was used at a concentration of 1 μM, which did not inhibit APA, but prevents degradation of the substrate by aminopeptidases such as B, N, and W and cytosolic aminopeptidases (34, 35). The rate of substrate hydrolysis was calculated for an equivalent level of expression for each mutant. Statistical comparisons were performed with Student's unpaired *t* test. Differences were considered significant if p was <0.05.

RESULTS

Modeling of APA—The alignment of the LTA_4H and APA sequences used for homology modeling is presented in Fig. 1*A*. Fig. 1*B* presents the structure of the entire protein, showing its organization into three domains: the N-terminal domain consisting mainly of β-sheets, the globular active-site domain, and the C-terminal helical domain. The N- and C-terminal domains have a large interface in common. The active site was found to be located in the middle of this interface and to be accessible from the outside (Fig. 1*C*).

The APA active-site structure obtained in the presence of the inhibitor glutamate phosphonate is presented in Fig. 2. The

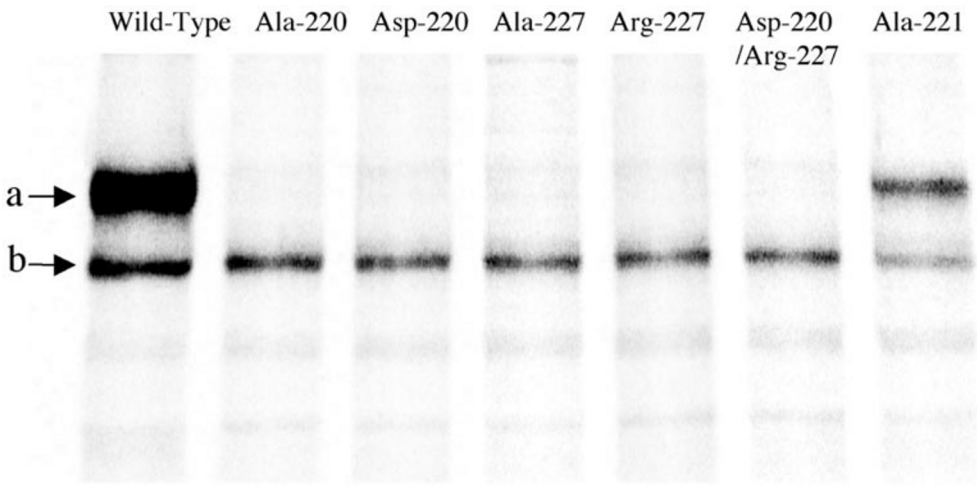

FIG. 4. **Metabolic labeling of histidine-tagged recombinant APAs.** Transiently transfected CHO cells were treated with G418 for 10 days. Cells were then labeled by incubation for 5 h with a [^{35}S]methionine/cysteine mixture, and cell lysate proteins were immunoprecipitated with a monoclonal anti-His_5 antibody, resolved by 5% SDS-PAGE, and identified by autoradiography. The *first* and *last lanes* correspond to wild-type His-APA and the Ala-221 control mutant, respectively. They each displayed two immunoprecipitated forms, 168 and 140 kDa in size. The other lanes correspond to the other mutants, which displayed only the 140-kDa form. For all the recombinant His-APAs, the signal corresponding to the non-glycosylated 110-kDa form was weak, but detectable.

organization of the active site obtained after refining the model was very similar to that observed in the LTA_4H complex (Fig. 2) (the residual mean square deviation between all heavy atoms of all the residues involved in or around the active site is only ~1.20 Å). The Zn^{2+} ion is hexacoordinated in the model. 1) The three active-site residues His-386, His-389, and Glu-408 in APA (which correspond to the three residues binding the zinc atom in LTA_4H: His-295, His-299, and Glu-318, respectively) are located in positions similar to those of their counterparts in LTA_4H. In the APA model, the two oxygen atoms of the Glu-408 carboxylate side chain coordinated the zinc ion. 2) One of the oxygen atoms of the phosphate of the inhibitor also contributes to the coordination sphere, as does a water molecule from the solvent.

A strong network of hydrogen bonds is kept stable around the zinc coordination sphere: the water molecule bound to the zinc ion is frozen in position during molecular dynamics, as it is also engaged in two conserved hydrogen bonds with the Glu-386 and Glu-352 side chains. The Glu-352 side chain is also hydrogen-bonded to the amine moiety of the inhibitor. His-385 (His-295 in LTA_4H) is also maintained in place by the engagement of its $N^{\delta 1}$ in a NH–CO hydrogen bond with the carbonyl group of Glu-415 (Glu-325 in LTA_4H). The phenol ring of Tyr-471 has a location in APA similar to that of the corresponding Tyr-383 in LTA_4H, and its hydroxyl group is hydrogen-bonded to an oxygen atom of the phosphate group of the inhibitor.

Other interactions within the APA chain may be important for the catalytic process and for the enzyme stability, but not immediately involved in the chemical activity of the molecule. For example, a salt bridge interaction between Asp-227 and Arg-220 appears to be important for the positioning of Glu-215 in the vicinity of the active site. This example is illustrated in Fig. 3*B*, showing that the Glu-215 side chain interacts by hydrogen bonding with the nitrogen group of the glutamate phosphonate inhibitor (a similar interaction was also found for bestatin). This Asp-227–Arg-220 salt bridge interaction is reinforced by another salt bridge, Arg-220–Asp-87, which kept the arginine guanidinium sandwiched between two carboxylate groups throughout the MD simulations. These interactions seem to be necessary to maintain the cohesion of the N-terminal β-sheet domain, especially the position of loop 215–230 inserted into the β-sheet organization of the N-terminal domain: this hairpin loop at residues 215–230 has a short helical portion at the top, and this short helical fragment closely interacts within the cavity formed by the strands (Fig. 3*C*). If both the Arg-220 and Asp-227 residues are replaced with Ala, and 500 ps of molecular dynamics simulations are run on the new system, the organization of the β-strand of the N-terminal domain is found to be greatly disturbed (residual mean square deviation of 6 Å on the C^{α} atoms of residues 79–280 between wild-type and mutant APAs *versus* 2.1 Å for the C-terminal domain residues). Similar behavior was observed if the Arg-220–Asp-227 pair was replaced with Asp-220-Arg-227, due to strong repulsion between the carboxylate groups of Asp-87 and the new Asp-220. This Asp-227–Arg-220 salt bridge therefore appears to be a possible test case for measuring the validity of the proposed models, as its disruption should destabilize the folding of the N-terminal domain surrounding the active site.

Site-directed Mutagenesis of His-APA cDNA—The mouse APA model revealed an interaction between Arg-220 and Asp-227 via a salt bridge that was necessary for the correct folding of the N-terminal domain. Alignment of the sequence of mouse APA with those of other monozinc aminopeptidases for the region located upstream from the zinc-binding motif HE*XX*H showed that these two residues are strictly conserved (Fig. 3*A*). To characterize these structural residues, we replaced Arg-220 with alanine or aspartate and Asp-227 with alanine or arginine by site-directed mutagenesis. We also switched these two residues to yield the Asp-220/Arg-227 double mutant. The non-conserved lysine residue at position 221 was also replaced with alanine as a control. Transiently transfected CHO cells producing wild-type and mutant His-APAs were labeled by incubation with [^{35}S]methionine/cysteine for 5 h and then lysed in detergent buffer, and His-APAs were immunoprecipitated with an anti-His_5 antibody. The immunoprecipitates were analyzed by SDS-PAGE and autoradiography (Fig. 4). The autoradiographs of wild-type APA and the Ala-221 control mutant displayed two bands, 168 and 140 kDa in size, corresponding to specifically immunoprecipitated proteins. The Ala-220, Asp-220, Ala-227, Arg-227 and Asp-220/Arg-227 APA mutants produced only the lower molecular mass form of the enzyme.

Mutant APAs Display Incorrect Maturation and Trafficking—We investigated whether the conserved Arg-220 and Asp-227 residues are important for the correct processing of the enzyme in the secretory pathway by performing metabolic

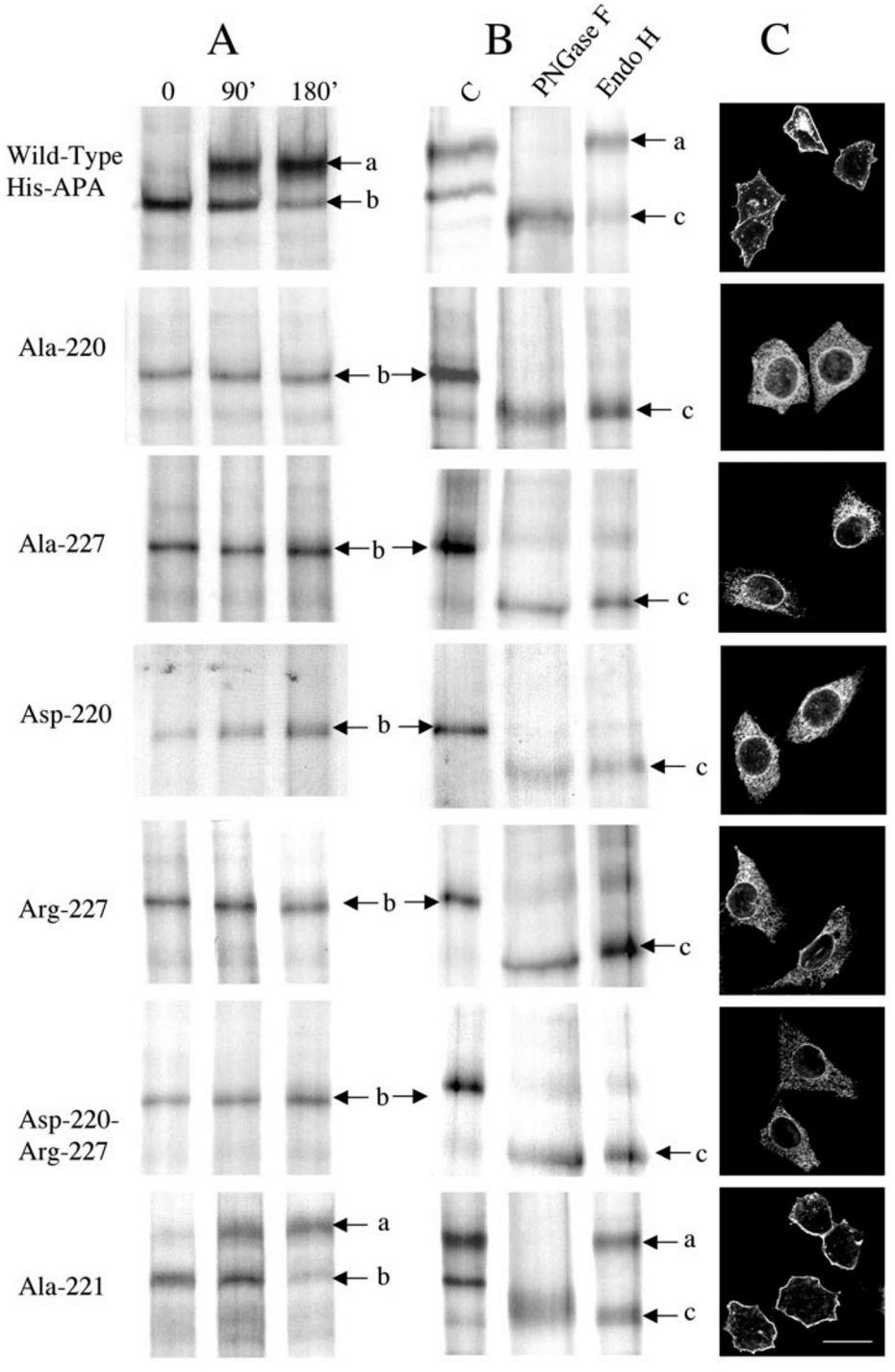

FIG. 5. **Maturation and expression of histidine-tagged recombinant wild-type and mutant mouse APAs.** *A*, CHO cells transiently producing wild-type APA and mutant APAs (Ala-220, Asp-220, Ala-227, Arg-227, Asp-220/Arg-227, and Ala-221) were labeled for 30 min with [^{35}S]methionine/cysteine and subjected to chase periods with serum-free medium for various lengths of time. Solubilized cell lysate proteins were immunoprecipitated with a monoclonal anti-His_5 antibody, resolved by 5% SDS-PAGE, and identified by autoradiography. The letters correspond to the 168-kDa form sorting from the Golgi apparatus (*a*) and the 140-kDa form sorting from the endoplasmic reticulum (*b*). *B*, after 90 min of chase, solubilized cell lysate proteins were immunoprecipitated with a monoclonal anti-His_5 antibody and treated with PNGase F or Endo H. Samples were subjected to 5% SDS-PAGE and identified by autoradiography. The letters correspond to the 168-kDa form sorting from the Golgi apparatus (*a*), the 140-kDa form sorting from the endoplasmic reticulum (*b*), and the 110 kDa non-glycosylated form (*c*). *C*, cells were fixed and immunolabeled with a rabbit polyclonal anti-rat APA serum and detected with a cyanin-3-conjugated anti-rabbit antibody. Immunofluorescence was detected by confocal microscopy. *Bar* = 20 μm.

labeling and pulse-chase experiments on wild-type and mutant His-APAs (Fig. 5*A*). Metabolic labeling and pulse-chase experiments on wild-type APA and the Ala-221 control mutant revealed a single immunoprecipitated band with an apparent molecular mass of 140 kDa after 30 min of pulse and a second band of 168 kDa after 90 min of chase. In contrast, the same experiment performed on mutant APAs revealed the presence of only a 140-kDa immunoprecipitated band, even after 180 min of chase.

PNGase F and Endo H Treatment of Wild-type and Mutant His-APAs—We further investigated the pattern of maturation and the intracellular location of wild-type and mutant APAs by treating cell lysates with PNGase F or Endo H. Treatment of glycoproteins with PNGase F removes all *N*-linked oligosaccharide side chains. Treatment with Endo H removes immature, but not medial Golgi-processed *N*-linked oligosaccharide side chains. Treatment with PNGase F was used as a positive control for deglycosylation of His-APAs. Treatment of wild-type His-APA and the Ala-221 control mutant with PNGase F led to the disappearance of both the 168- and 140-kDa forms of the proteins. Treatment of the mutant enzymes led to the disappearance of the 140-kDa form of these mutant proteins. For each recombinant APA, PNGase F treatment yielded one band, 110 kDa in size. For wild-type APA and the Ala-221 control mutant, the 140-kDa form was Endo H-sensitive and shifted to 110 kDa upon treatment, whereas the 168-kDa form was Endo H-resistant. The other mutant APAs displayed only the lower 140-kDa form of the protein, which was Endo H-sensitive and

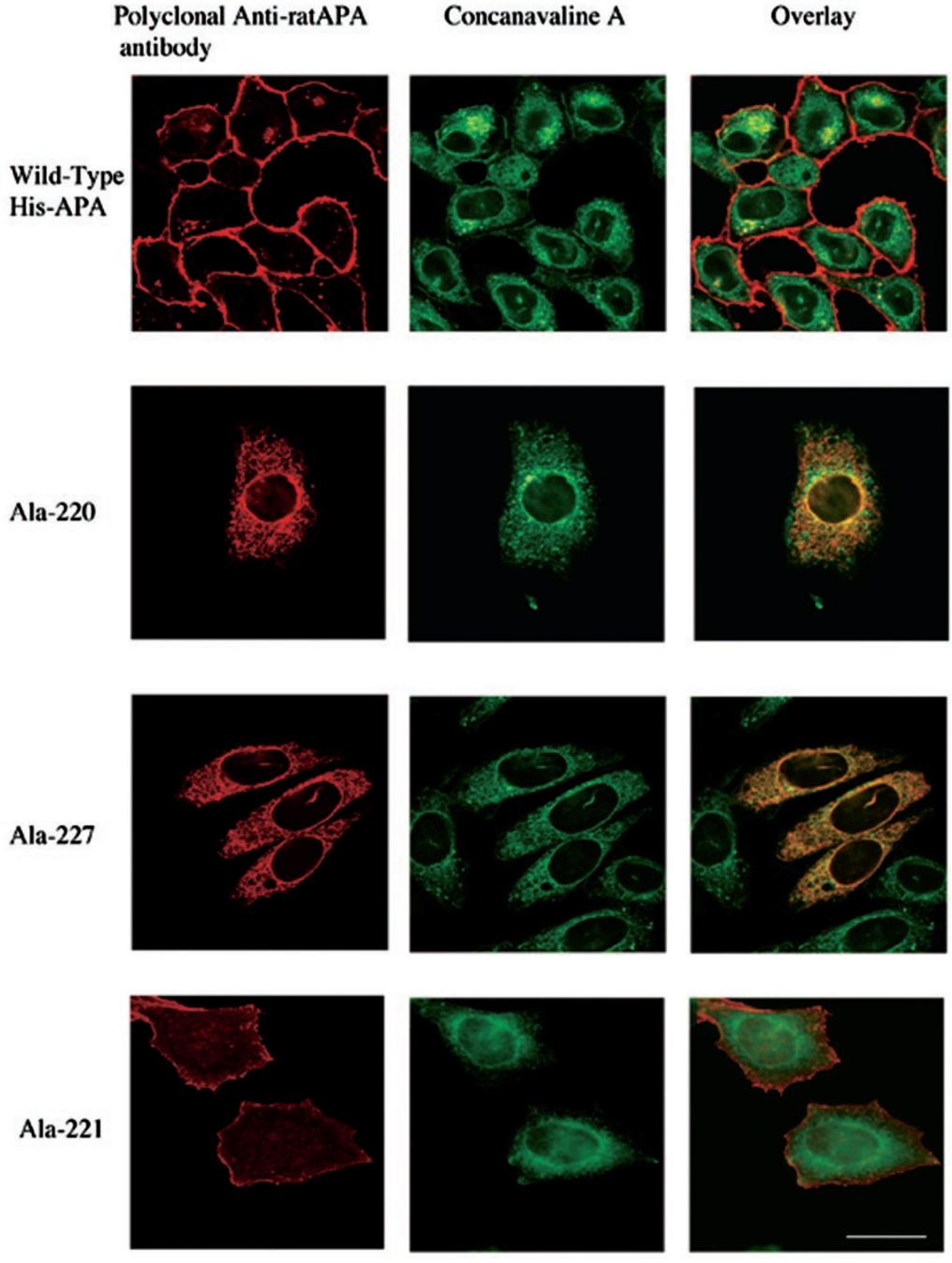

FIG. 6. **Double labeling of APA and concanavalin A.** Cells transiently producing wild-type APA and mutant APAs (Ala-220, Ala-227, and Ala-221) were fixed and immunolabeled with a rabbit polyclonal anti-rat APA serum. Labeling was detected by incubation with a cyanin-3-conjugated anti-rabbit antibody. Fluorescein-conjugated concanavalin A was added together with the secondary antibody. Immunofluorescence was observed by confocal microscopy. *Bar* = 20 μm.

shifted to 110 kDa upon treatment (Fig. 5*B*).

Immunofluorescence Labeling of Transiently Transfected Wild-type and Mutant APAs—We investigated the trafficking of wild-type and mutant APAs by performing immunofluorescence analysis with a rabbit polyclonal anti-rat APA antibody and a cyanin-3-conjugated anti-rabbit secondary antibody. Confocal microscopy analysis of CHO cells producing wild-type His-APA or the Ala-221 control mutant showed that APA was located in the plasma membrane. In contrast, the labeling pattern in cells producing the other mutant proteins showed that these mutant proteins were located within the cell and not in the plasma membrane (Fig. 5*C*). To identify further the compartment in which these mutant proteins were located, we carried out a double labeling experiment with fluorescent concanavalin A, a lectin that specifically binds to mannose-rich carbohydrate cores in glycoproteins and labels the ER. Confocal microscopy analysis of CHO cells producing wild-type His-APA or the Ala-221 control mutant showed different distributions for APA and concanavalin A. The cyanin-3 (*red*) labeling of APA was restricted to the plasma membrane, whereas fluorescein (*green*)-conjugated concanavalin A labeling was detected in the ER and the perinuclear cisterna of the cells. In contrast, the location of the Ala-220 and Ala-227 mutant His-APAs almost exactly matched that of the ER marker, consistent with these mutants being located in the ER compartment (Fig. 6).

Enzymatic Activity of His-APAs—We determined the enzymatic activity of cellular extracts of CHO cells transiently producing wild-type His-APA or the Ala-220 and Ala-227 mu-

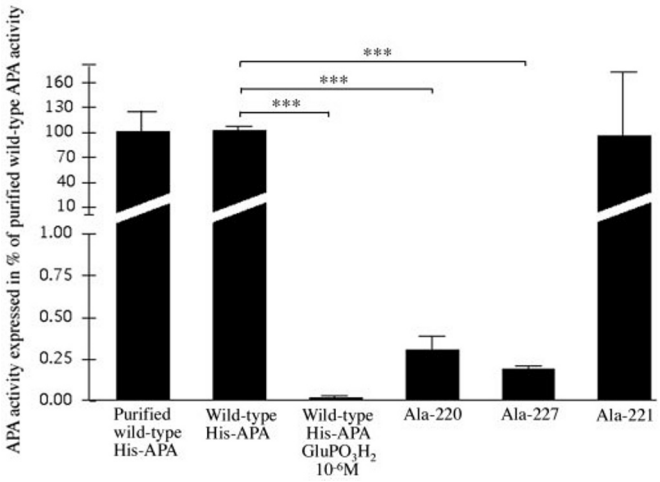

FIG. 7. **Enzymatic activity of histidine-tagged recombinant wild-type and mutant APAs.** Activities of wild-type APA and mutant APAs (Ala-220, Ala-221, and Ala-227) in cellular extracts of transiently transfected CHO cells are expressed as a percentage of purified wild-type activity. Activity assays were performed in the presence of 1 μM bestatin. The activity of wild-type APA in cellular extract was also determined in the presence of 1 μM glutamate phosphonate (*GluPO$_3$H$_2$*). Measurements are the means ± S.E. of three independent transfections with duplicate determinations. ***, $p < 0.001$. The mean value for purified wild-type APA corresponds to 83.4 nmol of substrate hydrolyzed per min/μg of purified APA.

tant His-APAs as a percentage of purified recombinant wild-type His-APA activity, taking into account the fact that equivalent amounts of recombinant enzyme were used, as described under "Experimental Procedures" (Fig. 7). Wild-type His-APA activity was abolished completely in the presence of 10^{-6} M glutamate phosphonate, a specific and selective inhibitor of APA, a generous gift from Dr. B. Lejczak. In contrast to what was observed for wild-type His-APA, the level of enzymatic activity detected for the Ala-220 and Ala-227 mutants was very low, corresponding to 0.30 and 0.18% of wild-type His-APA activity, respectively. The activity of wild-type His-APA, measured under the same assay conditions in transiently transfected cells, was also completely abolished in the presence of 10^{-6} M glutamate phosphonate.

DISCUSSION

As the crystal structure of APA has not yet been solved, site-directed mutagenesis studies have been used to investigate the organization of the APA active site (16–19, 25, 29). The recent resolution of the x-ray crystal structure of human LTA$_4$H (27), a bifunctional zinc metalloenzyme with both epoxide hydrolase and aminopeptidase activities, has provided an opportunity to construct models of other members of this metalloprotease family: gluzincins, and particularly monozinc aminopeptidases such as APA. In this study, we generated a molecular model of the mouse APA ectodomain (amino acids 79–559) using the human LTA$_4$H structure as a template. We also docked the inhibitor glutamate phosphonate, an analog of the transition state, into the active site of this model. The structure of the APA ectodomain deduced from this model was compared with the structures of LTA$_4$H and with the organization of the APA active site proposed on the basis of results of previous site-directed mutagenesis studies. The model demonstrated the crucial structural role of two conserved residues, Arg-220 and Asp-227. Site-directed mutagenesis of these residues was used to validate the model. The mutant proteins lacked enzymatic activity and were retained in the endoplasmic reticulum, demonstrating the importance of these amino acids for the correct folding and trafficking of APA, thereby confirming the structural role of these residues suggested by the model.

The structure of APA obtained from the model is folded into a flat triangle composed of three different domains: the N-terminal domain consisting mainly of β-sheets, the globular active-site domain, and the C-terminal helical domain. The N- and C-terminal domains have a large interface in common. The active site is located in this interface and is accessible from the outside. The organization of the active site is very similar to that observed in LTA$_4$H. Within the active site and particularly in the zinc-binding region, the structures of the two enzymes can be superimposed, suggesting a common structural feature in the monozinc aminopeptidase family.

In the three-dimensional model of APA, the zinc atom is coordinated by the two histidine residues (His-385 and His-389) of the HE*XX*H motif, consistent with the results obtained by Wang and Cooper (16). The zinc atom is also coordinated by a water molecule and Glu-408, which was shown by Vazeux *et al.* (17) to be the third zinc ligand. Similar ligation of the zinc atom in the active site of LTA$_4$H was observed with the equivalent residues in this enzyme (His-295, His-299, and Glu-318). The APA model also showed an interaction between Glu-415 (the equivalent of Glu-325 in LTA$_4$H) and His-385. The hydrogen bond between the side chain of the acidic glutamate and the protonated nitrogen HN$^{\delta 1}$ atom of the imidazole ring of His-385 (the equivalent of His-295 in LTA$_4$H) could function both by maintaining the position of the histidine side chain relative to the zinc ion and by polarizing the histidine N$^{\delta 2}$ atom, thereby increasing the strength of zinc coordination (36). This suggests that Glu-415 of APA may be functionally equivalent to Asp-991 in angiotensin-converting enzyme, Asp-170 in thermolysin, and Asp-650 in neutral endopeptidase 24.11, all of which are located in the conserved motif E*XXX*D and have been shown to play a role in positioning the first histidine (His-959 in angiotensin-converting enzyme, His-142 in thermolysin, and His-583 in neutral endopeptidase 24.11) of their respective zinc-binding motif HE*XX*H (26, 37, 38). In addition, the distance between the third zinc ligand and this acidic residue is conserved among the gluzincin family (four residues in angiotensin-converting enzyme, thermolysin, and neutral endopeptidase 24.11 and seven residues in APA, LTA$_4$H, and other monozinc aminopeptidases), suggesting a common functional role for this residue in monozinc aminopeptidases.

We then docked a potent and selective APA inhibitor, glutamate phosphonate, into the active site. It has been suggested that this compound binds to APA by interacting with the S1 subsite specific for N-terminal acidic amino acid residues and with the anionic binding site Glu-352. This inhibitor also behaves as a transition state analog in which the replacement of the substrate scissile amide bond with a phosphonic acid group mimics the tetrahedral transition state (28). One of the phosphoryl oxygens ligates the zinc in a tetrahedral complex and forms a hydrogen bond with Tyr-471 that is involved in transition state stabilization (18). The three-dimensional model of APA complexed with glutamate phosphonate provides evidence that the N-terminal amine of the inhibitor interacts with Glu-352 of APA as proposed by Vazeux *et al.* (19) and as proposed by Luciani *et al.* (21) for aminopeptidase N. The model also demonstrates an interaction between Glu-215 (the equivalent of Gln-136 in LTA$_4$H) and the N-terminal amine of the inhibitor. A similar interaction has been observed between Gln-136 of LTA$_4$H and the N-terminal amine of the co-crystallized inhibitor bestatin. However, site-directed mutagenesis studies on this residue resulted in no definitive conclusions (22), perhaps because LTA$_4$H is not strictly an aminopeptidase.

Studies of the docking of glutamate phosphonate also make

it possible to investigate interactions between the active site and the substrate during the catalysis step. Our data show that one of the phosphoryl oxygen atoms of the inhibitor binds the zinc atom, with another binding the water molecule. Glu-352 also binds the water molecule via a hydrogen bond. All these interactions are involved in control of the positioning of this water moiety, allowing Glu-386 to polarize the water molecule, promoting nucleophilic attack of the peptide bond. This interaction between Glu-386 and the water molecule was previously described by Vazeux *et al.* (17), who suggested that this residue is the catalytic effector of APA. In addition, the interaction between Glu-352 and the water molecule shown by the model may account for the large decrease in the catalytic constant following the mutation of this residue or equivalent residues in other enzymes (21, 22). The water molecule is not present in the active site of LTA_4H complexed with bestatin. This is probably due to the nature of bestatin, which does not display a conformation of an analog of the transition state. In addition, the phenol ring of Tyr-471 of APA (equivalent of Tyr-383 in LTA_4H) interacts with a phosphonic hydroxyl group of the inhibitor. This residue, shown to be essential for stabilizing the transition state of catalysis in aminopeptidase A (18), would be the counterpart of Tyr-149 in astacin (39, 40). In summary, these data are consistent with the catalytic model proposed on the basis of studies of the co-crystallization of thermolysin with various inhibitors (26) and with the catalytic model we proposed for APA (25).

This model also enabled us to identify residues essential to maintenance of the structure of APA. We identified two residues (Arg-220 and Asp-227) that seem to play a critical structural role by interacting with each other via a salt bridge and that seem to be necessary for maintaining the cohesion of the N-terminal β-sheet domain, therefore ensuring the correct folding of the N-terminal domain surrounding the active site. Indeed, if either of these two residues was replaced by alanine in the model, we observed severe perturbation of the structure of the N-terminal β-sheet domain, with a residual mean square deviation of 6 Å on the C^{α} atoms of residues 79–280 between wild-type APA and the Ala-220 and Ala-227 mutants. Similarly, site-directed mutagenesis of either of these residues resulting in their replacement with alanine resulted in the biosynthesis of mutant enzymes that were processed incorrectly. In pulse-chase experiments, cells producing wild-type APA and the Ala-221 control mutant displayed a 140-kDa form after 30 min of pulse and a 168-kDa form after 90 min of chase. The glycosylated groups of this high molecular mass form of APA were digested by PNGase F, but not by Endo H. Thus, this high molecular mass molecule corresponds to the mature glycosylated complex sorting from the Golgi apparatus. In contrast, the Ala-220 and Ala-227 mutants displayed only the lower molecular mass band (140 kDa), even after 3 h of chase. As this form of APA was digested by both Endo H and PNGase F, it probably corresponds to the immature high-mannose form of APA found in the ER.

Immunofluorescence experiments on wild-type and mutant His-APAs confirmed these results by showing that wild-type APA and the Ala-221 control mutant were present in the plasma membrane, whereas the Ala-220 and Ala-227 mutant APAs were present in an intracellular compartment. This pattern of localization was observed in transfected fibroblast CHO cells and corticotroph pituitary AtT20 cells (data not shown), suggesting that the pattern of maturation and trafficking is not related to the cell type, but is specifically related to the enzyme structure itself. In each case, we assessed the specific effect of the mutation because the Ala-221 control mutant displayed the same pattern of maturation and localization as wild-type APA. The colocalization of the Ala-220 and Ala-227 mutants, but not of wild-type APA, with concanavalin A in double labeling immunofluorescence experiments provides additional evidence that the recombinant mutant APAs are retained in the ER. This retention in the ER, in contrast with the plasma membrane location of wild-type APA, is consistent with the incorrect folding of mutant enzymes, which are then retained by the quality control mechanisms of the cell (41). We investigated the interaction between Arg-220 and Asp-227 further by creating a model for a double mutant in which Arg-220 and Asp-227 were inverted (Asp-220/Arg-227). This mutant protein behaved similarly to the Ala-220 and Ala-227 single mutant proteins, suggesting that the inverted residues do not interact with each other. We observed a strong repulsion between the carboxylate group of Asp-87 and the inverted Asp-220 residue, preventing the interaction between Asp-220 and Arg-227. We assessed the effect of this inversion in a cellular system using site-directed mutagenesis to generate the Asp-220 and Arg-227 single mutants and the Asp-220/Arg-227 double mutant. All these recombinant mutant proteins displayed the same pattern of maturation and trafficking as Ala-220 and Ala-227, as shown by the detection of a single 140-kDa Endo H-sensitive band in pulse-chase experiments and the ER retention observed by confocal immunofluorescence microscopy. These data are consistent with those collected in our model, showing that these two residues interact with each other via a salt bridge, which seems to be important for the correct folding of the N-terminal β-sheet domain.

In this work, we created a three-dimensional model of the major part of the APA ectodomain using the structure of LTA_4H as a template. This three-dimensional model of the APA ectodomain was found to be highly consistent with the organization of the APA active site proposed on the basis of previous mutagenic studies. The three-dimensional model of APA revealed the presence of two residues (Arg-220 and Asp-227) that appeared to be critical to the structure of the protein, interacting with each other via a salt bridge. This salt bridge was necessary for maintenance of the cohesion of the N-terminal β-sheet domain and therefore for the correct folding of the N-terminal domain surrounding the active site. We validated this model by site-directed mutagenesis. We demonstrated that the mutant APAs were incorrectly maturated, localized within the cell, and lacked enzymatic activity, confirming the structural role of these residues. This model is therefore a powerful new tool for further investigation of the active site of APA and for designing new inhibitors of the enzyme that could be used as central antihypertensive agents.

REFERENCES

1. Nagatsu, I., Nagatsu, T., Yamamoto, T., Glenner, G. G., and Mehl, J. W. (1970) *Biochim. Biophys. Acta* **198,** 255–270
2. Wilk, S., and Healy, D. (1993) *Adv. Neuroimmunol.* **3,** 195–207
3. Lodja, Z., and Gossrau, R. (1980) *Histochemistry* **67,** 267–290
4. Zini, S., Masdehors, P., Lenkei, Z., Fournie-Zaluski, M. C., Roques, B. P., Corvol, P., and Llorens-Cortès, C. (1997) *Neuroscience* **78,** 1187–1193
5. Chauvel, E. N., Llorens-Cortès, C., Coric, P., Wilk, S., Roques, B., and Fournié-Zaluski, M. C. (1994) *J. Med. Chem.* **37,** 2950–2956
6. Zini, S., Fournié-Zaluski, M. C., Chauvel, E., Roques, B. P., Corvol, P., and Llorens-Cortès, C. (1996) *Proc. Natl. Acad. Sci. U. S. A.* **93,** 11968–11973
7. Reaux, A., Fournie-Zaluski, M. C., David, C., Zini, S., Roques, B. P., Corvol, P., and Llorens-Cortès, C. (1999) *Proc. Natl. Acad. Sci. U. S. A.* **96,** 13415–13420
8. Reaux, A., Fournie-Zaluski, M. C., and Llorens-Cortès, C. (2001) *Trends Endocrinol. Metab.* **12,** 157–162
9. Wu, Q., Lahti, J. M., Air, G. M., Burrows, P. D., and Cooper, M. D. (1990) *Proc. Natl. Acad. Sci. U. S. A.* **87,** 993–997
10. Li, L., Wang, J., and Cooper, M. D. (1993) *Genomics* **17,** 657–664
11. Nanus, D. M., Engelstein, D., Gastl, G. A., Gluck, L., Vidal, M. J., Morrison, M., Finstad, C. L., Bander, N. H., and Albino, A. P. (1993) *Proc. Natl. Acad. Sci. U. S. A.* **90,** 7069–7073
12. Troyanovskaya, M., Jayaraman, G., Song, L., and Healy, D. P. (2000) *Am. J. Physiol.* **278,** R413–R424
13. Hesp, J. R., and Hooper, N. M. (1997) *Biochemistry* **36,** 3000–3007

14. Jongeneel, C. V., Bouvier, J., and Bairoch, A. (1989) *FEBS Lett.* **242,** 211–214
15. Hooper, N. M. (1994) *FEBS Lett.* **354,** 1–6
16. Wang, J. Y., and Cooper, M. D. (1993) *Proc. Natl. Acad. Sci. U. S. A.* **90,** 1222–1226
17. Vazeux, G., Wang, J., Corvol, P., and Llorens-Cortès, C. (1996) *J. Biol. Chem.* **271,** 9069–9074
18. Vazeux, G., Iturrioz, X., Corvol, P., and Llorens-Cortès, C. (1997) *Biochem. J.* **327,** 883–889
19. Vazeux, G., Iturrioz, X., Corvol, P., and Llorens-Cortès, C. (1998) *Biochem. J.* **334,** 407–413
20. Papadopoulos, T., Kelly, J. A., and Bauer, K. (2001) *Biochemistry* **40,** 9347–9355
21. Luciani, N., Marie-Claire, C., Ruffet, E., Beaumont, A., Roques, B. P., and Fournie-Zaluski, M. C. (1998) *Biochemistry* **37,** 686–692
22. Rudberg, P. C., Tholander, F., Thunnissen, M. M., and Haeggstrom, J. Z. (2002) *J. Biol. Chem.* **277,** 1398–1404
23. Kull, F., Ohlson, E., Lind, B., and Haeggstrom, J. Z. (2001) *Biochemistry* **40,** 12695–12703
24. Laustsen, P. G., Vang, S., and Kristensen, T. (2001) *Eur. J. Biochem.* **268,** 98–104
25. Iturrioz, X., Rozenfeld, R., Michaud, A., Corvol, P., and Llorens-Cortès, C. (2001) *Biochemistry* **40,** 14440–14448
26. Matthews, B. W. (1988) *Acc. Chem. Res.* **21,** 333–340
27. Thunnissen, M. M., Nordlund, P., and Haeggstrom, J. Z. (2001) *Nat. Struct. Biol.* **8,** 131–135
28. Lejczak, B., Choszczak, M. P. D., and Kafarski, P. (1993) *J. Enzyme Inhib.* **7,** 97–103
29. Iturrioz, X., Vazeux, G., Celerier, J., Corvol, P., and Llorens-Cortès, C. (2000) *Biochemistry* **39,** 3061–3068
30. Herlitze, S., and Koenen, M. (1990) *Gene* (*Amst.*) **91,** 143–147
31. Laemmli, U. K. (1970) *Nature* **227,** 680–685
32. Song, L., Ye, M., Troyanovskaya, M., Wilk, E., Wilk, S., and Healy, D. P. (1994) *Am. J. Physiol.* **267,** F546–F557
33. Chauvel, E. N., Coric, P., Llorens-Cortès, C., Wilk, S., Roques, B. P., and Fournié-Zaluski, M. C. (1994) *J. Med. Chem.* **37,** 1339–1346
34. Schalk, C., d'Orchymont, H., Jauch, M. F., and Tarnus, C. (1994) *Arch. Biochem. Biophys.* **311,** 42–46
35. Tieku, S., and Hooper, N. M. (1992) *Biochem. Pharmacol.* **44,** 1725–1730
36. Li, G. S., Maigret, B., and Ruiz-Lopez, M. F. (1998) *J. Comp. Chem.* **19,** 1675–1688
37. Williams, T. A., Corvol, P., and Soubrier, F. (1994) *J. Biol. Chem.* **269,** 29430–29434
38. Oefner, C., D'Arcy, A., Hennig, M., Winkler, F. K., and Dale, G. E. (2000) *J. Mol. Biol.* **296,** 341–349
39. Grams, F., Dive, V., Yiotakis, A., Yiallouros, I., Vassiliou, S., Zwilling, R., Bode, W., and Stocker, W. (1996) *Nat. Struct. Biol.* **3,** 671–675
40. Yiallouros, I., Grosse Berkhoff, E., and Stocker, W. (2000) *FEBS Lett.* **484,** 224–228
41. Hammond, C., and Helenius, A. (1995) *Curr. Opin. Cell Biol.* **7,** 523–529
42. Bradford, M. M. (1976) *Anal. Biochem.* **72,** 248–254